FERMILAB-PROPOSAL -0916 916

Further Studies in Hard Diffraction and Very Forward Physics

The CDF Collaboration

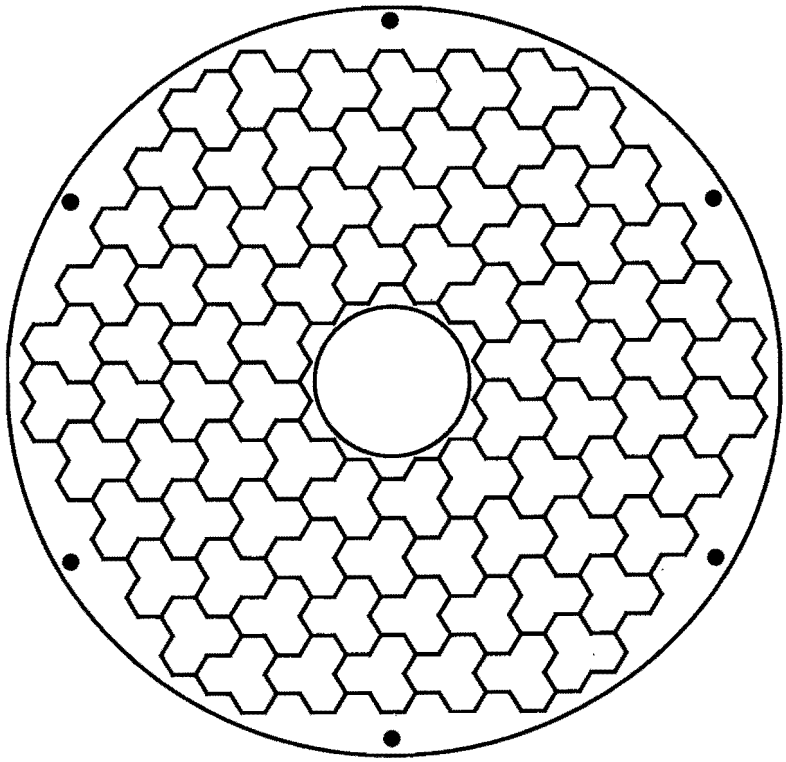

October 4, 1999

SUMMARY

We propose a program of studies in hard diffraction and very forward physics with CDF in Run II, which requires the **Roman Pot Spectrometer (RPS)** used in Run 1C to detect leading antiprotons, adding to CDF two forward **MiniPlug** calorimeters to cover the region $3.5 < |\eta| < 5.5$, and installing a set of **Beam Shower Counters (BSC)** around the beam pipe at four (three) locations along the $\bar{p}$ (p) beam direction to tag rapidity gaps within $5.5 < |\eta| < 7.5$.

In Run 1C, the $\bar{p}$-beam was behind the proton beam, as viewed from the RPS side. An inverted polarity (with respect to Run I) of the electrostatic beam separators will enable us to move the RPS detectors closer to the $\bar{p}$-beam and thereby gain acceptance down to $\xi \equiv 1 - x_{\bar{p}} = 0.03$, where the cross section is dominated by pomeron exchange (in Run 1C the range covered was $0.05 < \xi < 0.1$).

The MiniPlugs will be placed within the holes of the muon toroids. A MiniPlug prototype of a unique design has been constructed and tested in high energy muon, electron and pion beams with excellent results. The MiniPlugs will have an $\eta - \phi$ segmentation and, in addition to measuring the energy could, if upgraded with additional electronics, provide accurate position resolution not only for electrons and photons but also for hadrons. Used as rapidity gap detectors, the MiniPlugs will extend the ξ-coverage below the region covered by the Roman Pots and, combined with the Plug, down to $\xi \sim 0.005$.

Some of the physics topics we plan to address with these detectors are:

- **Hard single diffraction:** W, heavy flavor and dijet production; dependence of the cross section on ξ and t; third-jet activity in jet production (probing the quark/gluon nature of the pomeron); extraction of the pomeron structure function.
- **Soft and hard double diffraction (central rapidity gaps):** dependence of cross section of dijet events with a rapidity gap between jets on jet E_T and jet η separation; measurement of soft double diffraction cross section and comparison of rapidity gap fractions in minimum bias and in dijet events.
- **Double pomeron exchange (DPE):** Measurement of dijet and exclusive cross sections in pomeron-pomeron collisions; measurement of soft DPE cross section; tests of soft and hard factorization; connection between soft and hard diffractive processes; opportunities for new physics (glueballs?).
- **Small-x/large-x physics:** Measurement of proton PDFs in the range $4 \times 10^{-5} < x < 0.8$; x_{max} can be measured as a function of the E_T scale down to E_T of 5 GeV.
- **Search for Centauros and Disoriented Chiral Condensates (DχC):** The signature for Centauros/DχCs is multiparticle clusters of large $dN/d\eta$ with abnormal charge to neutral ratios.
- **The MiniPlugs as a luminosity monitor:** The MiniPlug calorimeters can provide a reliable luminosity monitor, which complements the features of and can be used in parallel with the Čerenkov Luminosity Counters (CLC).

1 Introduction

In the past few years the field of diffraction has experienced a renaissance. Experiments at $p\bar{p}$ Colliders and at HERA have been probing the diffractive structure function of the proton, shedding light on the intricate interplay between soft and hard diffraction. While a firm *QCD based* theoretical interpretation of the experimental results is still lacking, the wealth of the accumulated experimental data allows questions to be asked about the factorization properties of the diffractive structure function of the proton and the uniqueness of the pomeron structure.

At HERA, the structure of the pomeron has been probed in studies of events with a rapidity gap produced in ep collisions at $\sqrt{s} \sim 300$ GeV. Such "gap events" are presumed to be produced in collisions between a virtual photon, emitted by the electron, and a virtual pomeron, emitted by the proton, as shown in Fig. 1. The gap (absence of particles) arises from the nature of the pomeron, which is colorless and carries the quantum numbers of the vacuum.

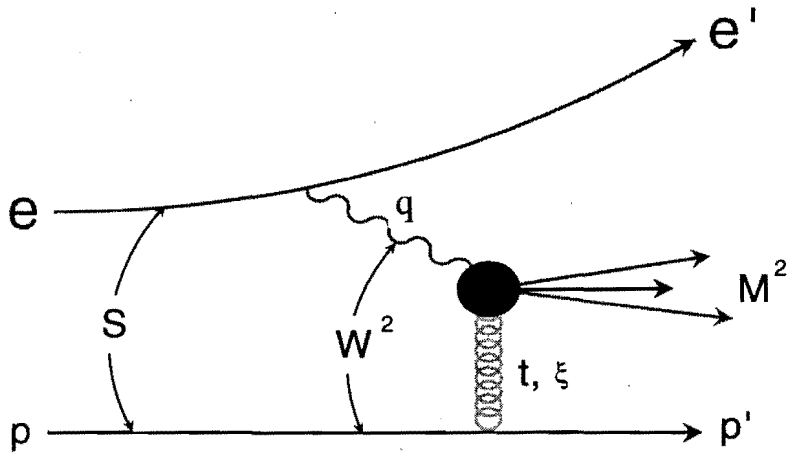

Figure 1: Schematic diagram of a diffractive DIS collision involving a virtual photon, emitted by an electron, and a virtual pomeron, emitted by a proton.

The HERA experiments have provided accurate measurements of the diffractive structure function of the proton through studies of diffractive Deep Inelastic Scattering (DIS), the traditional way of measuring structure functions. Recently, both the H1 and ZEUS experiments at HERA have added to their detectors Roman Pot leading particle spectrometers, which are used to measure the momentum of the forward proton and thereby provide a more accurate measurement of the momentum of the pomeron than that provided by the width of the rapidity gap.

The diffractive structure function measured in DIS, F_2^D, is defined through the equa-

tion for the DIS cross section

$$\frac{d^4\sigma}{dQ^2\,d\beta\,d\xi\,dt} = \frac{4\pi\alpha^2}{\beta Q^4}\left(2 - 2y + \frac{y^2}{2(1+R)}\right)\cdot F_2^{D(4)}(Q^2,\beta,\xi,t) \tag{1}$$

In addition to the standard DIS variables,

$$Q^2 = -q^2 \quad x_{bj} = \frac{Q^2}{2\,q\cdot p} \quad y = \frac{q\cdot p}{e\cdot p} \quad W^2 = (q+p)^2 \quad s = (e+p)^2 \tag{2}$$

the following variables are used for *diffractive* DIS:

$$\beta = \frac{Q^2}{2\,q\cdot(p-p')} = \frac{Q^2}{M_X^2 + Q^2 - t} \quad \xi = \frac{q\cdot(p-p')}{q\cdot p} = \frac{M_X^2 + Q^2 - t}{W^2 + Q^2 - m_p^2} \tag{3}$$

Note that $x_{bj} = \beta\xi$, so that β, which is used in place of x_{bj}, may be interpreted as the fraction of the momentum of the pomeron carried by the scattered parton.

From Fig. 1, it is seen that the diffractive structure function is the product of the pomeron structure function, $F_2^{I\!P}(Q^2,\beta)$, and the probability for pomeron emission by the proton, $f_{I\!P/p}(s,Q^2,\beta\xi,t)$, which is also referred to as the "pomeron flux". Under the assumption of a *universal* pomeron flux that depends only on ξ and t, $f_{I\!P/p}(\xi,t)$, the Q^2 and β dependence of $F_2^{D(4)}$ would be that of the pomeron. However, such a universal flux fails to describe the soft $\bar{p}p$ diffractive cross section [1]. This is one reason why it is important to study the diffractive structure function not only in DIS at HERA, but also at $\bar{p}p$ colliders. In fact, it has been shown [2, 3] that predictions for hard diffraction cross sections at the Tevatron based on the diffractive structure function measured at HERA are generally $\sim$ 10 times larger than the measured values. This breakdown of factorization has been traced back [2] to a breakdown of pomeron flux factorization in soft diffraction. Thus, a quantitative understanding of the structure of the pomeron requires an understanding of both soft and hard diffractive processes.

At CDF, we have studied both soft and hard diffraction. In the 1989 Run, we measured the elastic [4], diffractive [5] and total [6] $\bar{p}p$ cross sections at $\sqrt{s} = 546$ and 1800 GeV. In Runs 1A and 1B, we studied hard diffraction using the rapidity gap technique to tag diffractive events [7, 8, 9, 10, 11, 12]. Finally, in Run 1C (1995-96), using a Roman Pot Spectrometer to detect the leading antiproton, and two small calorimeters to act as rapidity gap detectors in the very forward region, we studied dijet events produced in single diffraction dissociation, as well as dijets produced in pomeron-pomeron collisions (hard double-pomeron exchange).

Below, we summarize briefly our results on hard diffraction, state our physics goals for Run II, discuss the detector components to be added to CDF, and present our plans for implementing the proposed program.

2 Summary of Run I Results on Hard Diffraction

There are two sets of results on hard diffraction obtained from the analysis of Run I data using two different methods to tag diffraction: the rapidity gap technique (Runs 1A and 1B), and a Roman Pot Spectrometer that detected the recoil antiproton and measured its momentum (Run 1C).

Figure 2 shows the diagram of a single diffractive (SD) collision and the resulting event topology.

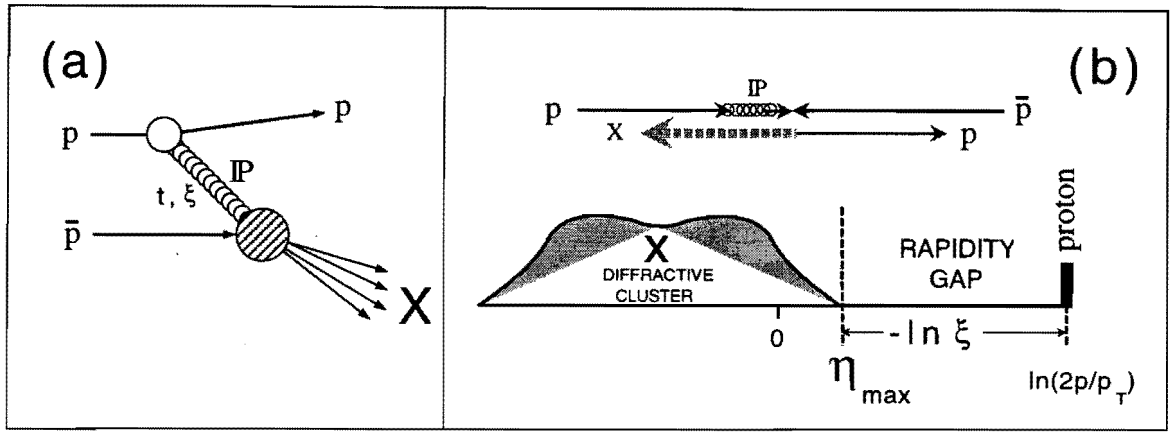

Figure 2: (a) Schematic diagram and (b) event topology for $p\bar{p}$ diffraction dissociation.

In Run I, the rapidity gap method for tagging single diffractive events had good acceptance at low ξ-values, where pomeron exchange is dominant, but provided no measurement of the pomeron momentum. In contrast, the Roman Pot technique provided a good measurement of the momentum of the pomeron, but had good acceptance only at relatively high ξ, where other (reggeon) exchanges also contribute substantially.

Figure 3 shows the topology for single diffraction (SD), double diffraction (DD), and double-pomeron exchange (DPE).

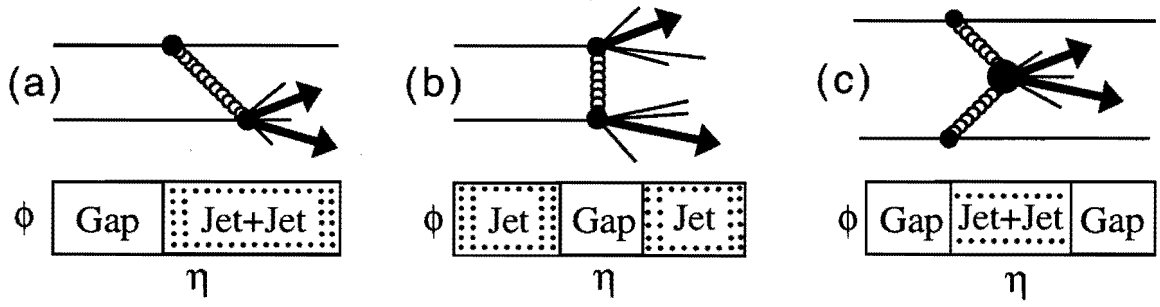

Figure 3: Schematic diagrams showing (a) single diffraction, (b) double diffraction, and (c) and double pomeron exchange processes and their topologies.

All three processes were studied in CDF. Our results are summarized below.

2.1 Hard diffraction studies using rapidity gaps

1. **Diffractive W production.**
   Status: Published in Phys. Rev. Letters [7].
   Comments: We measured the fraction of W events produced diffractively and compared the measured ratio with predictions based on the diffractive structure function measured at HERA. Using the standard pomeron flux, we found that factorization fails; our result agrees with the renormalized flux prediction [1].

2. **Diffractive dijet production.**
   Status: Published in Phys. Rev. Letters [8].
   Comments: We measured the fraction of diffractive to non-diffractive events with two jets of $E_T^{jet} > 20$ GeV in the region of $\eta > 1.8$ or $\eta < 1.8$. By comparing the measured rate with that for diffractive W production, we determined the gluon fraction of the pomeron. This result agrees with the result of ZEUS obtained by comparing the rates of DIS and dijet production in photoproduction. The CDF and ZEUS results on the gluon fraction are independent of the pomeron flux normalization. However, a factorizable process-independent pomeron flux cannot account for both measured *rates*, indicating a breakdown of factorization.

3. **Dijet production by color-singlet exchange at 1800 GeV.**
   Status: Published in Phys. Rev. Letters [9].
   Comments: We measured the fraction of events with two jets of $E_T^{jet} > 20$ GeV, one in the region $1.8 < \eta < 3.5$ and the other within $-3.5 < \eta < -1.8$. The measured fraction agrees with our previous measurement based on the 1989 data and with the value measured by DØ. We found no appreciable dependence of the rapidity gap fraction on jet E_T, but observed an intriguing fall-off at large rapidity separation between the jets.

4. **Dijet production by color-singlet exchange at 630 GeV.**
   Status: Published in Phys. Rev. Letters [10].
   Comments: We found that the fraction of gap events increases with decreasing energy: $R_{gap}(630/1800) = 2.4 \pm 0.9$. In this PRL, we also presented the gap fraction at $\sqrt{s} = 1800$ GeV as a function of the momentum fractions of the partons in the p and $\bar{p}$, x_p or $x_{\bar{p}}$ (two entries per event). The gap fraction was found to be flat in x, indicating that the ratio of the color singlet effective coupling to the color octet coupling is similar for quarks and gluons.

5. **Diffractive b-quark production.**
   Status: Submitted to PRL.
   Comments: The diffractive to non-diffractive ratio was found to be $[0.62 \pm 0.19(stat) \pm 0.16(syst)]\%$ for electrons from b-decay in the range $|\eta^e| < 1.1$ and $9 < E_T^e < 20$ GeV.

6. **Diffractive J/Ψ production**
   Status: Analysis nearly complete; preliminary results reported at conferences.

2.2 Hard diffraction studies using roman pots

In our diffractive studies using the rapidity gap technique, we were successful in observing and measuring the rate of production of W-bosons, dijets, b-quarks and J/Ψ's. However, the rates alone do not *uniquely* specify the pomeron structure. A straightforward way to extract the pomeron structure is by using the kinematic variables in diffractive dijet events, provided the pomeron momentum is known. Using the RPS in Run 1C, we determined the pomeron momentum by measuring the momentum of the leading antiproton.

1. **Diffractive dijets at 630 and 1800 GeV.**
   Status: Analysis for 1800 GeV completed, PRL draft ready; analysis for 630 GeV in progress.
   Comments: We measured the diffractive structure function of the $\bar{p}$ and compared it with expectations based on HERA measurements. We find a softer structure and rates lower by a factor of ~ 10. The observed breakdown of factorization is quantified as a function of $x(\bar{p})$.

2. **Double-pomeron dijets at 1800 GeV.**
   Status: Analysis complete; PRL draft in preparation.
   Comments: We observed a clear signal of double pomeron exchange dijet events and made the first measurement of the double-ratio of DPE to diffractive over diffractive to non-diffractive dijet events, which we use to test factorization.

The diffractive physics program of Run I has/will produce six Ph.D. theses:

1. Diffractive W production
   Suren Bagdasarov (Rockefeller) [graduated]

2. Roman Pot dijets at 630 GeV
   Kenichi Hatakeyama (Rockefeller)

3. Diffractive J/Ψ production
   Andrei Solodsky (Rockefeller)

4. Diffractive *b*-quark production
   Hirofumi Ikeda (Tsukuba) [graduated]

5. Roman Pot dijets at 1800 GeV
   Hosai Nakada (Tsukuba)

6. Double pomeron exchange dijets
   Koji Terashi (Tsukuba)

3 Physics Goals for Run II

Our main goal for Run II is to understand the nature of the pomeron and determine its partonic structure. We also plan to investigate new areas of forward physics, such as probing the small/large-x gluon content of the proton through forward dijet production and searching for exotic phenomena of the centauro and disoriented chiral condensate type.

3.1 Single Diffraction Dissociation (SDD)

In Run 1C, the antiproton spectrometer had good acceptance in the region of $0.05 < \xi < 0.1$. In this region, there are substantial contributions from sub-leading Regge trajectories. To ensure pomeron dominance, lower ξ-values are necessary. The average ξ of our rapidity gap dijet signal was 0.015. However, no accurate measurement of the ξ-value was possible from the width of the rapidity gap using the BBC and forward calorimeter information.

Using the RPS, with the polarity of the Tevatron electrostatic beam separators inverted (with respect to Run I), we will cover the range $0.03 < \xi < 0.1$, while using the MiniPlug and Plug Upgrade calorimeters to actually *measure* the rapidity gap, we will cover the range $0.005 < \xi < 0.03$, without requiring special running conditions. Thus, we expect to have continuous coverage in the region $0.005 < \xi < 0.1$.

3.2 Double Diffraction Dissociation (DDD)

The $\Delta\eta$ dependence of the ratio of dijet events with a rapidity gap between jets to non-gap events probes the coupling of the exchanged color-singlet object to quarks and gluons relative to the coupling of the normal color-octet exchange. For a $2 \rightarrow 2$ process, the pseudorapidities of the jets of a given E_T are related to the x-values by

$$x_1 = \frac{E_T^{jet}}{\sqrt{s}}\left(e^{\eta_1} + e^{\eta_2}\right) \qquad x_2 = \frac{E_T^{jet}}{\sqrt{s}}\left(e^{-\eta_1} + e^{-\eta_2}\right) \tag{4}$$

For $E_T = 20$ GeV, $x = 1$ corresponds to $\eta = 4.6$ (for $\sqrt{s} = 2$ TeV), which is the MiniPlug central η-value. Thus, the MiniPlugs will be important in studying the nature of hard color-singlet exchange interactions by allowing a comparison of the relative color-singlet to color-octet couplings as a function of the x-value of the parton in the proton all the way up to $x \approx 1$.

Using the MiniPlugs, we will also make accurate measuremennts of *soft* DDD, the process in which both the proton and antiproton dissociate. This process is characterized by a rapidity gap between two clusters of particles at the regions of high rapidity. The cross section for DDD can be compared with the standard and renormalized [1] Regge theory predictions and with predictions of other models [13]. Also, the ratio of DDD to minimum bias (MB) events may be compared with the same ratio for events with jets. Such a comparison is crucial to understanding the mechanism of the survival probability of the rapidity gap in events with jets [14].

3.3 Double Pomeron Exchange (DPE)

Hard pomeron-pomeron (DPE) collisions are by far the most exotic and interesting hard diffraction process. In Run I, we observed ~ 100 DPE dijet events using a combination of an antiproton tag and a rapidity gap tag on the proton side. In Run II, the MiniPlugs will be used to tag rapidity gaps, while the total pomeron-pomeron c.m.s. energy will be measured using the Central and Plug calorimeters.

Using the Plug Upgrade and MiniPlug calorimeters, we can study low mass DPE (large rapidity gaps on each side). The mass of a central cluster of rapidity width Δy is given by $M \approx e^{0.5\,\Delta y}$. Thus, for rapidity gaps starting at $|\eta| = 1.1$ ($|\eta| = 5$), M is 3 (150) GeV. One measurement of interest is the soft DPE cross section as a function of central mass M. Another interesting area of physics is the search for exclusive states produced in $I\!P - I\!P$ collisions, e.g. glueballs or $Q\bar{Q}g$ hybrids.

3.4 Small-x/large-x physics

Both the small-x and large-x regions of the proton structure function are of great interest. These regions can be investigated by measuring the cross section of events with two jets in the forward region. As seen in Eq. (4), the x-value of the interacting partons can be obtained from the jet η for a given E_T^{jet}. Small-x values are probed using same-side (SS) dijet events with the two jets at the same side of η ($\eta_1\eta_2 > 0$), while large-x values can be probed with either SS or opposite-side (OS) jets ($\eta_1\eta_2 < 0$). At $\sqrt{s} = 2$ TeV, the minimum and maximum $x-$values that can be reached for dijets of $E_T^{jet} = 5$ GeV are

$$x_{min} \simeq 4 \times 10^{-5} \qquad x_{max} \simeq 0.4\,(0.8) \text{ for SS (OS) dijets} \tag{5}$$

The dijet events probe the parton density and do not discriminate between gluons and quarks. The large-x gluon density of the proton can be probed using events with a prompt (isolated) photon in the central region and a jet in the MiniPlug. Such events will most likely be due to the collision of a large-x gluon with a low-x quark.

3.5 Centauros and Disoriented Chiral Condensates (DχC)

The unique signature for centauro or DχC type events is high multiplicity of relatively low P_T clusters of particles depositing predominately hadronic or electromagnetic energy. A search for such events has already been performed in the minimum bias CDF data of Run 1A [15, 16] with negative results. The fine segmentation of the MiniPlugs, and the excellent position resolution they can provide not only for leptons and photons but also for hadrons, makes them ideal detectors for searching for centauro and DχC type events.

It has been proposed that centauro events are produced diffractively [17]. In Run II, we propose to trigger on high mass single diffractive events using the antiproton spectrometer and search for centauros in the plug and MiniPlug regions.

4 Beam Shower Counters (BSC)

In studying single diffractive (SD) and double-pomeron exchange (DPE) processes, which are characterized by forward rapidity gaps, an ideal rapidity gap tagger (RGT) at the trigger level would be one that rejects all non-diffractive and multiple interaction events, while retaining all diffractive ones. An almost ideal RGT can be realized by a set of *Beam Shower Counters* around the beam pipe at several locations along the $\bar{p}$ and p directions covering the pseudorapidity region $5.5 < |\eta| < 7.5$.

The reasons that make this η-coverage good for rapidity gap tagging are the following:

- For single diffractive events with a leading antiproton, the minimum pseudorapidity, η_{min} [1], that can be reached by a particle from the diffractive cluster is

$$\eta_{min} = \ln \frac{p_T}{2\xi p_0}$$

  where $p_0 = 1000$ GeV. For $< p_T >= 0.5$ GeV and $\xi < 0.05$, $\eta_{min} > -5.3$. Thus, the proposed RGT will retain almost all the diffractive events with $\xi < 0.05$. Since the $dN/d\eta$ of the diffractive cluster in the vicinity of η_{min} is small and can fluctuate to zero, a large fraction of diffractive events with ξ larger than 0.05 will also survive this veto.

  Simulations using the POMPYT Monte Carlo program show that for dijet events of $E_T^{jet} > 15$ GeV, the RGT retains $\sim 99\%$ of the single diffractive events that have a roman pot tag. The $\sim 1\%$ that are rejected have ξ-values in the vicinity of 0.1. For non-diffractive events, PYTHIA predicts that only $\sim 1\%$ of dijet events of $E_T^{jet} > 15$ GeV are retained. Since the ratio of diffractive to non-diffractive dijet production rates is $\sim 0.1 - 1\%$, requiring rapidity gaps in the trigger is a necessity rather than luxury.

- The RGT can also be used to veto non-diffractive minimum bias events. This is important for the inclusive Roman Pot and Double Pomeron Exchange triggers, and also for rejecting at the trigger level events due to multiple interactions. MBR simulations show that the fraction of non-diffractive events retained by a single-arm RGT is $\sim 3\%$, and the fraction retained by the double-arm RGT (in "AND") is $\sim 0.3\%$.

The proposed RGT can be realized by a BSC system consisting of four stations on the West and three on the East side of the detector, as shown in Fig. 4. The East side (p-direction) is symmetric to the West, except that it has no warm straight section in a location corresponding to that of the Roman Pots on the West side. Therefore, only three BSC stations can be installed on the East side.

A BSC station will consist of a layer of scintillation counters preceeded by a $3/8''$ thick lead plate to convert γ's. The output of each PMT will be directed to a CAFE card of an ADMEM board. This information will be read out for every CDF event for off-line

[1] η is negative in the antiproton direction, see Figure 2b.

studies. The BSCs will detect particles either directly from the interaction region or by the showers they produce by hitting the beam pipe and/or magnet walls. BSCs 2, 3 and 4 will consist of $6'' \times 6''$ scintillator plates with a hole in the center to accommodate the beam pipe. Each of these BSCs will be made of two halves and will be positioned so as to 'hug' the beam pipe. The two BSC-1's will be circular with a $4.75''$ OD and a $2.75''$ hole, and will be made of four quarters. These counters will also be used as "beam loss" monitors by the accelerator Beams Division. At the BSC-1 location the beam pipe has a diameter of $2.5''$, which can comfortably accommodate the $2.75''$ diameter hole of the BSC-1 assemblies. This BSC configuration will cover approximately the range $5.5 < |\eta| < 7.5$. The total number of BSC counters will be 18, 10 on the West side and 8 on the East side of the detector.

Using the proposed RGT will free the Miniplugs from the trigger, so that the Miniplug information can be used to evaluate ξ from the size of the rapidity gap.

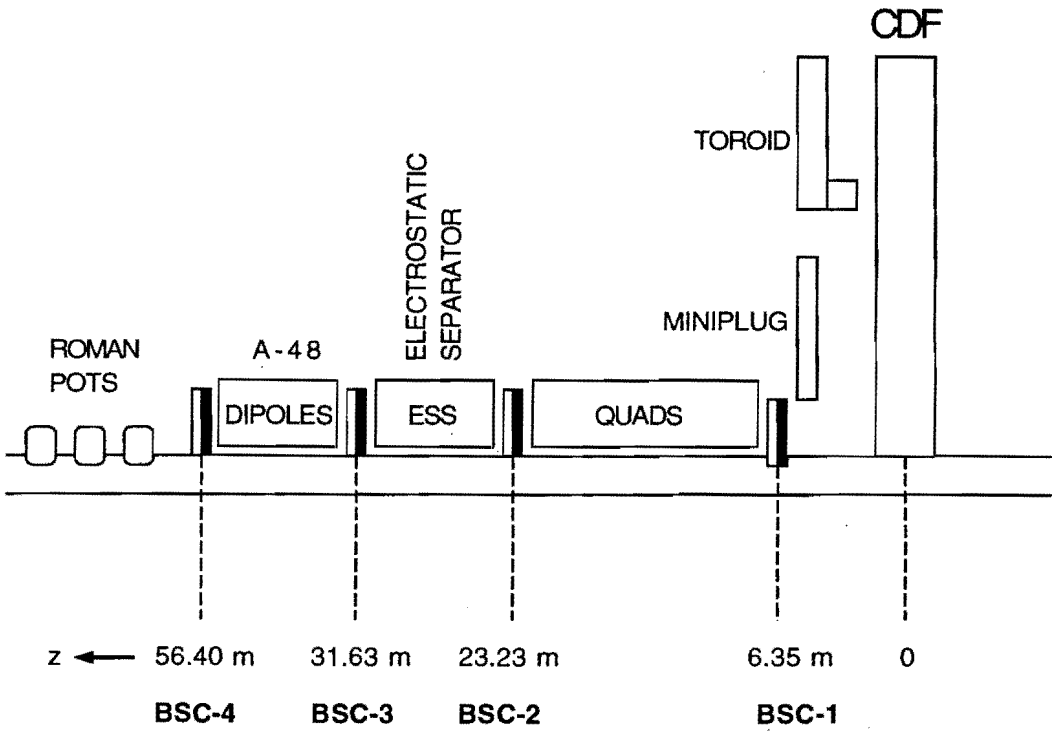

Figure 4: Location of the Beam Shower Counter stations along the $\bar{p}$ direction on the West side of CDF (not to scale). On the East side only the first three BSC stations will be installed, as there is no room for BSC-4.

5 Roman Pots

We propose to use the same detectors that were used in Run 1C to detect leading antiprotons. These detectors were placed in three Roman Pots located at the warm straight section of the Tevatron immediately after the A-48 string of dipole magnets, as shown in Fig. 5.

In Run 1C, the closest distance from the antiproton beam that the detectors could be brought to was $\sim$ 15 mm. At that distance, the spectometer had almost full acceptance in the region $0.05 < \xi < 0.1$ for $t = 0$, as indicated in Fig. 5. To extend the ξ-acceptance to lower ξ-values, and hence increase the ratio of pomeron to reggeon contribution to the cross section, requires bringing the detectors closer to the $\bar{p}$ beam. During Run 1C, the antiproton beam was further away from the Roman pots than the proton beam. The Beams Division has agreed to change the polarity of the electrostatic separators of the Tevatron [18] to enable us to bring the Roman Pots $\sim$5 mm closer to the antiproton beam and thereby access lower ξ-values. Fig.6 shows the (approximate) ξ, t acceptance of the Roman Pot Spectrometer for the detectors at a distance of 10 mm from the $\bar{p}$ beam. Details about the acceptance and ξ, t resolution can be found in CDF Note 2940 ("Proposal for Hard Diffraction Studies in CDF", January 1995).

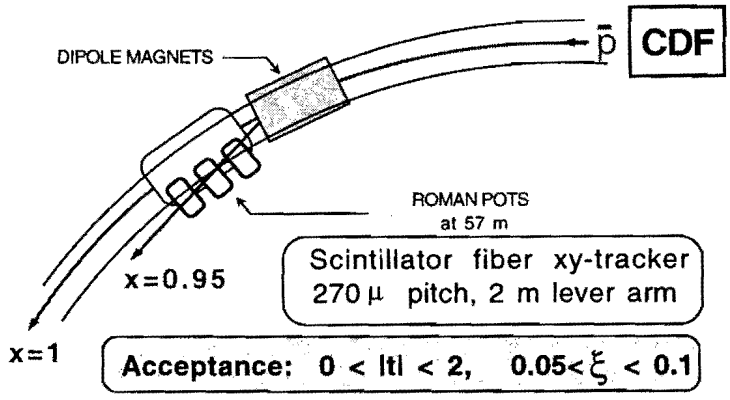

Figure 5: Schematic view of the Roman Pot Spectrometer in Run 1C.

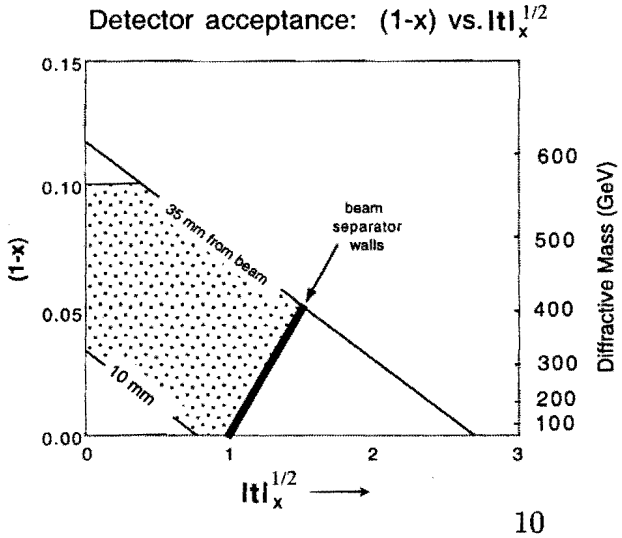

Figure 6: Roman Pot Spectrometer $\xi \equiv 1 - x_F$ and t acceptance in Run II. The shaded area shows the good acceptance region (see details in CDF Note 2940).

6 MiniPlugs

Fig. 7 shows one quadrant of the CDF–II configuration. We propose to install two MiniPlugs downstream of the Plug Upgrade calorimeters within the central holes of the muon toroids, at about 5.8 meters from the center of the detector. The MiniPlugs will cover about two units in pseudorapidity, extending the Plug coverage all the way down to the beam pipe.

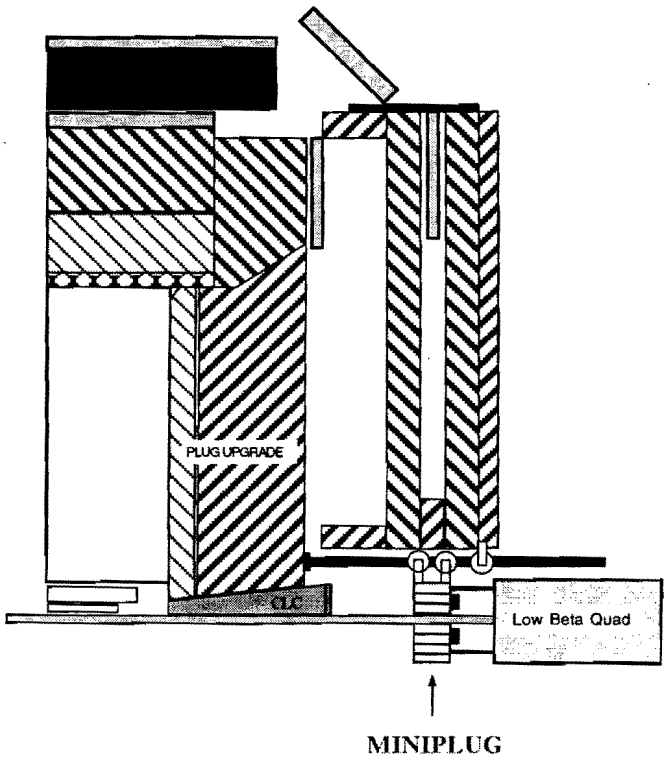

Figure 7: Schematic drawing showing a MiniPlug hanging from two beams supported on one end by the plug and on the other by the toroid (not to scale). This scheme allows for moving the toroids and/or the plug while the MiniPlug remains stationary.

The MiniPlug calorimeters are designed to measure charged and neutral hadron transverse energy, as well as pseudorapidity. The conceptual MiniPlug design and Monte Carlo predictions of its expected performance at high energies have been described in a CDF Note [19] and in the proceedings of an international conference on calorimetry [20]. Results obtained with the prototype MiniPlug calorimeter tested with 2, 3 and 5 GeV electron beams and an 8 GeV π^- beam at the Brookhaven National Laboratory (BNL) in 1994 were reported in a CDF Note [21], at an international conference on calorimetry [22], and in a NIM publication [23]. The prototype was also tested with high energy electrons and pions in the 1997 Fermilab test beam, and the results were reported in a CDF Note [24], at two international conferences [25, 26], and in a paper published by NIM [27]. The response of the prototype to positrons in the range 5–120 GeV and to charged pions in the range 10–230 GeV showed good linearity, to less than

1.5% for positrons and less than 4% for pions. For electromagnetic showers, we measured an energy resolution of σ/E = 18.1% / $\sqrt{E}$ + 0.6%. High precision measurements of the lateral position of both electromagnetic and hadronic showers were achieved with resolutions of 9.2 mm / $\sqrt{E}$ for positrons and 23.9 mm / $\sqrt{E}$ for pions. All 1997 Test Beam results were in good agreement with simulation predictions and with our BNL 1994 measurement at lower beam energies.

Below, we describe briefly the conceptual MiniPlug design and present the proposed MiniPlug design for CDF-II. Details on the MiniPlug optical system, radiation damage, GEANT simulation, calibration, and the effect on the nearby CDF detectors, mainly on the CMX muon chambers, can be found in the proposal presented by the proponents of this program to the CDF Collaboration [28].

6.1 Conceptual MiniPlug design

In 1994, we designed, constructed and tested a prototype "Pixel Array Detector" (PAD) calorimeter capable of determining the energy and, without using a shower maximum detector (SMD), the position of both electromagnetic and hadronic shower-initiating particles incident at small angles relative to the detector axis. A unique *towerless* geometry, combined with low cost construction, render the PAD suitable for "calorimetric tracking" of particles in the very forward region of collider detectors in moderate luminosity environments like that of CDF in Run II. This is the design we are now proposing for the calorimeters to be used in the very forward region of CDF for diffractive studies without, however, the high granularity that could be achieved by an eventual upgrade (additional electronics channels).

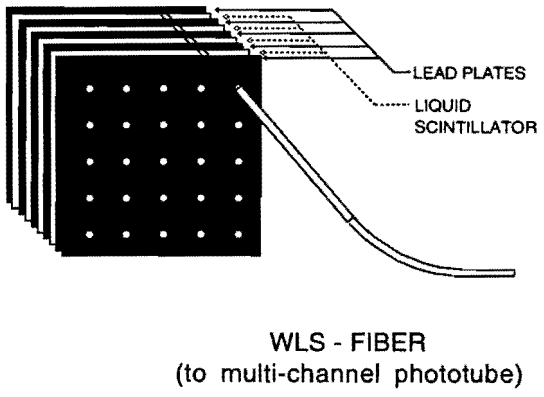

Figure 8: Conceptual design of a PAD calorimeter.

The PAD is a "shish-kebab" type calorimeter. It consists of alternating layers of lead plates and liquid scintillator read out by wavelength-shifting (WLS) fibers. The fibers are inserted into an array of aligned holes drilled in the lead plates as shown in Fig. 8 and are read out individually or in groups by multi-channel photomultiplier tubes (MCPMT's).

For particles incident at small angles relative to the fiber direction, the fiber pulse height centroid provides the position of the shower initiating particle. Position determination is obtained not only for electrons and photons but also for hadrons, which upon interaction release on average 1/3 of their energy in the form of π^0's.

6.2 The MiniPlugs proposed for CDF–II

Due to the space constraints in the z-direction when the Plug is in the "open" position, the length of the MiniPlug has to be confined to 24″. A schematic drawing of a side view of a 24″ long MiniPlug is presented in Fig. 9. In this design, the MiniPlug has 35 plates 25″ in diameter consisting of 3/16″ thick Pb sandwiched between 0.5 mm thick reflective Al sheets. The plates are separated by 1/4″ spacers and are immersed in liquid scintillator. Table 1 lists the properties of the materials of the MiniPlug.

Table 1: Properties of MiniPlug materials

Material	Rad. length (cm)	Int. length (cm)	Density (g cm^{-3})
Pb	0.56	17.1	11.36
Fe	1.76	16.8	7.87
Al	8.90	39.3	2.70
H_2O (liq. scint.)	36.08	84.9	1.00

Each plate is 0.86 radiation lengths (RL) and 0.03 interaction lengths (IL), and (taking into account the holes) weighs 16 Kg. The active length of a MiniPlug, including the liquid scintillator, is approximately 30 RL and 1.3 IL. The total weight of a MiniPlug is about 750 Kg (1650 lbs).

Figure 10 shows a Miniplug plate. The design is based on a hexagon geometry. Each hexagon has six holes, as shown. A WLS fiber is inserted in each hole. The six fibers of a hexagon are grouped together and are viewed by one MCPMT channel. There are 252 hexagons in each MiniPlug viewed by 18 16-channel MCPMTs. The MCPMT outputs are added in groups of 3 to form calorimeter "towers", which could eventually be read out individually. At this time we are only proposing to read out the summed MCPMT outputs (18 channels per MiniPlug).

The towers viewed by the three MCPMTs of a sextant are shown in Fig. 10 with different shades. In the MiniPlug prototype we used one 0.83 mm dia. fiber per cm^2, and grouped four fibers together to form a "tower" of effective area of 4 cm^2. In this design, there is one fiber per 1.6 cm^2, but we plan to use 1 mm dia. fibers to compensate for the reduction of light expected from the larger area covered by each fiber.

6.3 MiniPlug supports

In CDF-II, the MiniPlugs will be mounted within the holes of the toroids, as shown in Fig. 7. Each MP is hanging by rollers from two beams. One end of each beam is attached solidly to the plug and the other end is attached to a toroid half by rollers. The position of the MP is held fixed by a lightweight attachment to the low-β quad frame. This scheme allows for the toroid halves to be pushed back either simultaneously or one at a time, as desired; after the toroids are back, the plug can be pulled out. During these operations the MP remains stationary with its position stabilized by its attachment to the quad frame. The MiniPlug supports have already been designed and a full-scale prototype has been constructed and tested for deflections under a load of 2000 lbs.

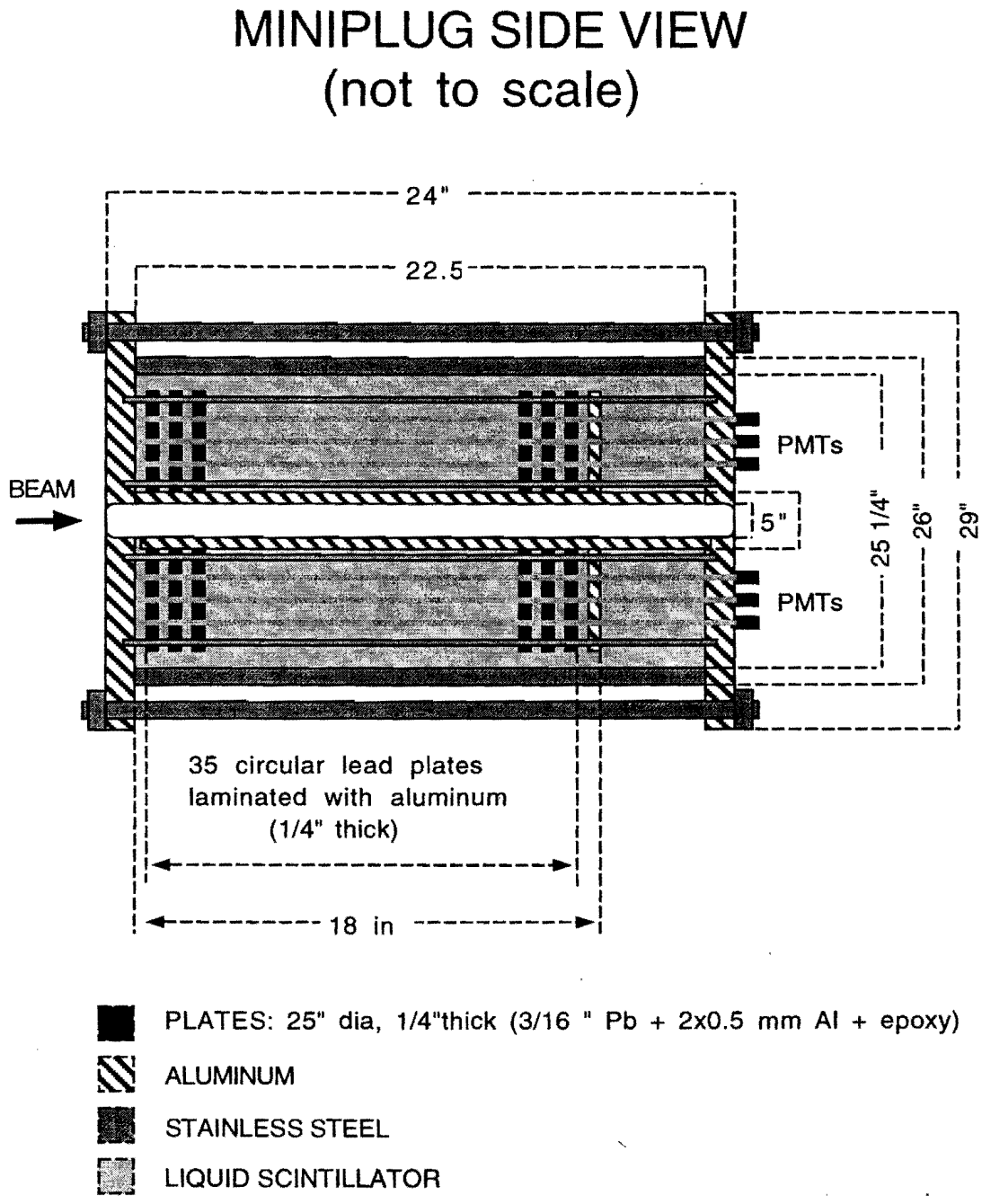

Figure 9: Schematic side view of a Miniplug.

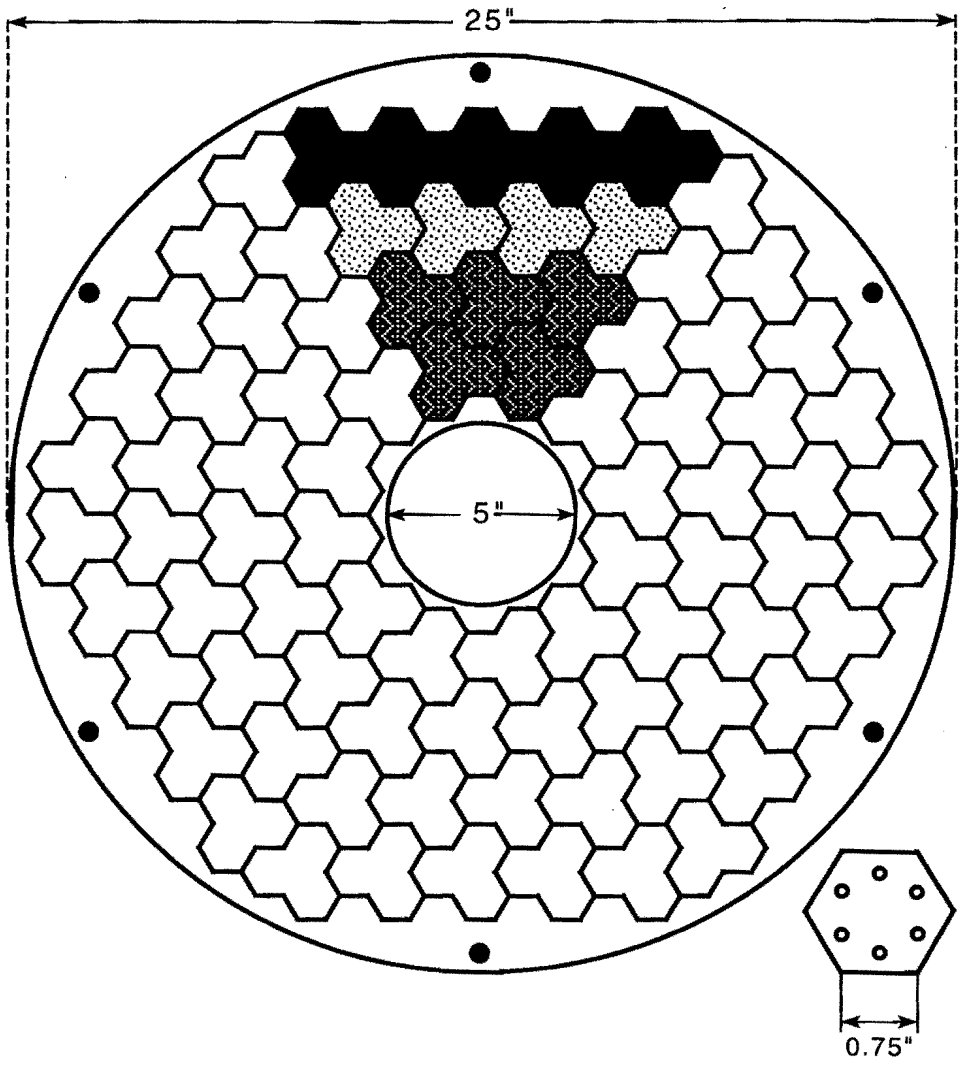

Figure 10: Proposed MiniPlug lead plate. The design is based on a hexagon geometry. Each hexagon has six holes, with a WLS fiber inserted in each hole. The six fibers of a hexagon are grouped together and are viewed by one MCPMT channel. There are 252 hexagons in each MiniPlug viewed by 18 16-channel MCPMTs. The MCPMT outputs are added in groups of 3 to form 84 calorimeter "towers".

6.4 MiniPlug read-out

We propose to use Bicron 517L liquid scintillator and Kuraray Y11 1.0 mm dia. WLS fibers read out by Hamamatsu R5900-M16 MCPMTs.

The Bicron 517L liquid scintillator, also used in the prototype, is a mineral oil with no particular safety requirements. Because of its high chemical compatibility with polystyrene based fibers, low cost and its radiation hardness, the BC-517L scintillator was studied for applications at SSC. The lifetime of BCF-91 WLS fibers immersed in BC-517L liquid scintillator was measured to be longer than 15 years [29].

In the prototype we used Kuraray Y11 0.8 mm WLS fibers. The use of larger diameter fibers can improve the resolution, as tests show that a 30% increase of light yield can be achieved by changing Kuraray Y11 0.8 mm dia. fibers to Kuraray Y11 1.0 mm dia. fibers [30].

The Hamamatsu R5900–M16, a 16 channel tube, was selected for the Plug Upgrade Shower Max Detector (SMD) because of its low cost per channel and its superior channel to channel gain uniformity. Developments in the Hamamatsu R5900 MCPMT family indicate that it is possible to achieve a quantum efficiency greater than 15%, which is adequate for the MiniPlug.

The expected radiation dose for the MiniPlug has been estimated to be $\approx$ 30 KGy (3 Mrad) per year in Run II. Such a dose is not expected to affect the response of the MCPMTs or of the liquid scintillator.

The borosilicate glass of the MCPMT window is more sensitive to radiation and in testing it showed a 60% relative transmittance at 500 nm for a similar dose. Hamamatsu is now able to provide R–5900 MCPMTs with a quartz window for improved radiation hardness and we already purchased five of them.

SSC studies on WLS fibers showed that the permanent damage of 1.0 mm dia., 1 m long fibers is about 10% after an irradiation of 64 KGy. Radiation hardness studies performed for LHC showed that Kuraray Y11 fibers were the least damaged when compared to other commercially available fibers.

We plan to use the same front end electronics as those used in the Plug Upgrade calorimeter.

7 Triggering and Data Acquisition

7.1 Level 1 inputs

The diffractive trigger will require seven (reserved) L1 inputs, as follows:

P	Pot (roman pot track candidate)
G_E, G_W	Gap (forward rapidity gap, East or West, from BSCs)
M_E, M_W	Miniplug signals, East and West
R1,R2	Two inputs reserved for future needs

7.2 Trigger table

The L1 triggers will be combined with hard triggers at L2, as shown in Table 2. This table includes some triggers that are of more general interest, such as the beam crossing trigger (X), an inclusive tower trigger (T), and single inclusive jet triggers with low, medium and high thresholds J_L, J_M and J_H, of order 10, 20 and 50 GeV. These triggers will also be needed for the non-diffractive low E_T jet studies and therefore we do not count them in the "diffractive budget". The trigger table is designed to give the maximum number of diffractive high-E_T jet events and $I\!P I\!P \to JJ$ events without prescaling. The thresholds are chosen to yield a rate of about 10^6 events per year in diffractive dijet production $J_L P$ and also in double pomeron exchange $GJJP$ (before off line selections, including multiple interaction rejections, about a factor about 10 altogether). Some of the triggers in Table 2 are also important for non-diffractive physics.

7.3 Comments

• The total rate of all diffractive triggers at $L = 1 \times 10^{32}$ cm^{-2} sec^{-1} is about 2 Hz, not including the proposed 0.5 Hz of Minimum Bias (X) triggers. This rate corresponds to 20 nb at L3.

• The beam crossing trigger X is prescaled at Level 1 to the agreed rate and goes straight through. We are proposing that this happen all the time at a constant *rate*.

Uses:

(a) studying the turn-ons of the next-more-restrictive trigger elements,

(b) as a large sample for MB→ soft diffraction→ the onset of hard diffraction studies,

(c) selecting single vertex events as a "standard candle" illuminating CDF's detectors.

• The roman pot trigger P goes into L1, where it is (a) heavily prescaled and passed through, and (b) put into AND with other L1 inputs, with lower or no prescaling.

• A rapidity gap G, defined by the anti-output of BSC_E or BSC_W, is a trigger element that must itself be studied, but it is common in X events and thus no special trigger is needed for G studies.

• Towers T are required for the non-diffractive jet studies and are not counted in the diffractive trigger budget.

• The J_H threshold is chosen to be the same as the non-diffractive threshold of 50 GeV. Requiring P at L1 reduces the needed prescaling factor to about 1. PJ_H should be

Table 2: The Diffractive Trigger

Trigger Name	Trigger Elements	Cross Section	Prescale Factor	L3 Rate (Hz)
Beam Crossing	X	(2.5×10^6)	5×10^6	(0.5)
Pot Inclusive	P	1 mb	2×10^5	0.5
Gap	G			
Tower	T			
E_T^{jet} >threshold (L, M, H)				
Jet-L (low thresholds)	J_L			
Jet-M (medium threshold)	J_M			
Jet-H (high threshold)	J_H			
Single Diffractive Jets				
SD Jet-L	$J_L P$	1μb	10^3	0.1
SD Jet-M	$J_M P$	50 nb	50	0.1
SD Jet-H	$J_H P$	1 nb	1	0.1
SD Jet-L $\oplus$ Gap	$J_L G$	2μb	10^3	0.2
SD Jet-M $\oplus$ Gap	$J_M G$	100 nb	50	0.2
SD Jet-H $\oplus$ Gap	$J_H G$	2 nb	1	0.2
SD J/ψ	$P\mu_1\mu_2$	?	?	0.1
SD $Q\bar{Q}$	$P\mu$	?	?	0.1
Double-$I\!P$ Exchange				
DPE-PG	$GJ_L P$	1 nb	1	0.1
DPE-GG	$GJ_L G$	1 nb	1	0.1
Very Forward				
SS=same-side, OS=opposite-side				
2 VF SS J_7	$M_E M_E$ or $M_W M_W$	1μb	10^3	0.1
2 VF OS J_7	$M_E M_W$	1μb	10^3	0.1
1 VF J_{20}	M_H	1μb	10^3	0.1
TOTAL RATE	$\sum$			2.1

about 1 nb and 0.1 s^{-1}. The J_M and J_L thresholds can be 20 GeV and 10 GeV to match the non-diffractive jet choices. The cross section for $GJ_L P$ will be about 1 nb.

• The MiniPlug 1-jet and 2-OS/SS-jet triggers are for studies of extremes in high and low-x, with and without rapidity gaps. The OS and SS triggers are extensions of the standard two-forward-jet triggers, which have smaller $|\eta|_{min}$ and larger $E_{T,min}$.

• Size of data sets: Assuming 10^7 seconds/year at an *average* luminosity of 10^{32} $cm^{-2}s^{-1}$ (1 fb^{-1}), the exclusively diffractive data set will be about 2×10^7 events. About 25% of these events, which are the pot-inclusive and those involving G, will be relatively small events, while the rest will be of typical size.

8 Schedule

An aggressive time schedule for constructing the two MiniPlugs by February 2000 is shown in Fig. 11.

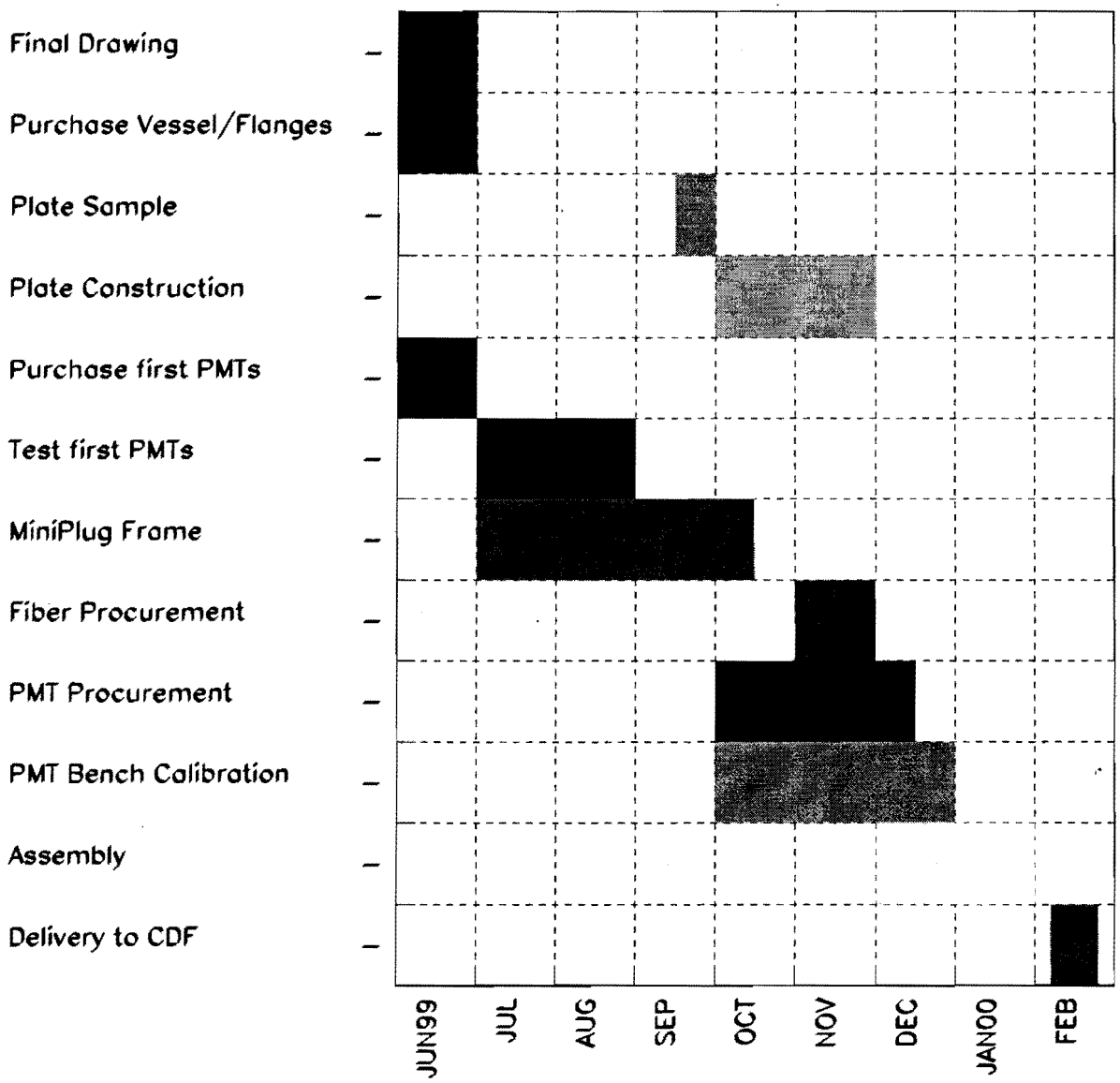

Figure 11: MiniPlug Schedule.

9 Cost estimate

A major part of the cost of the proposed three forward detector systems is the cost of the electronics. Most of the proposed physics program can be performed with the BSCs, the RPS and the 18-channel segmentation of the MiniPlugs provided by reading out only the sum-outputs of the MCPMTs. The design is such that the remaining physics (sections 3.4 and 3.5) can be addressed by simply adding more electronics channels to achieve higher granularity.

In allocating the cost among the BSC, RPS and MP systems, it is important to realize that the 18 BSC counters, the 3 RPS trigger counters and the 36 (sums of 16) MiniPlug MCPMT outputs use Plug electronics. The signals from all 57 channels will be sent to two VME crates: one located nearby the RPS, and the other, for MP and BSC counters, located on the first floor of the BØ building. A total of four ADMEM boards will be required to read all the channels.

9.1 Cost of BSC system

Table 3 summarizes the estimated cost of the BSC system. As mentioned previously, the BSC-1 counters will also be used as "beam loss" monitors by the accelerator Beams Division. The cost of special electronics that may be needed to provide signals to the accelerator control room is not included in this Table.

Table 3: BSC system

	Quantity	Unit Price	Cost	Funding Source
Counters	18		**10,000**	**ITEP**
PMT's	18		**20,000**	**Rockefeller**
ELECTRONICS				
CAFE card	18	120	2,160	
ADMEM board	1	3,200	3,200	
ADMEM transition board	1	300	300	
CAEN card and A932N	2	1,300	2,600	
Signal Cables	18		1,000	
HV Cables	18		1,000	
TOTAL Electronics			**10,260**	

9.2 Cost of Roman Pot Spectrometer

The existing Roman Pots and associated detectors need no modifications.

The readout system consists of a total of 240 MCPMT SciFi channels plus 3 trigger counter channels.

Shower-Max electronics will be used for the 240 SciFi channels. Five Shower-Max Digitizer (SMD) boards will be accomodated in a 6U SMD crate. One SMXR board will be placed in a 9U VME crate located near the SMD crate. One ADMEM board will be used for the trigger counters.

The cost of the RPS is given in Table 4.

Table 4: Roman Pot Spectrometer

	Quantity	Unit Price	Cost	Funding Source
Roman Pot Spectrometer			**150,000**	**Tsukuba**
SQUID card	60	120	7,200	
SMD board	5	770	3,850	
SMD transition module	5	125	625	
Signal cables (240 channels / 16)	15		1,250	
6U SMD Crate	1	600	600	
SMC Controller	1	850	850	
SMXR board	1	3,500	3,500	
SMXR Transition module	1	450	450	
Cable SMD-SMXR	5	100	500	
Cable SMC-SMXR	1	100	100	
Roman Pots Front-End			**18,925**	
Trigger Counter CAFE card	3	120	360	
ADMEM board	1	3,200	3,200	
ADMEM transition board	1	300	300	
9U VME Crate	1	4,300	4,300	
TRACER	1	1,400	1,400	
CPU	1	5,000	5,000	
Power Supply	1	6,000	6,000	
Complete VME Crate			**16,700**	
TOTAL Electronics			**39,485**	

9.3 Cost of MiniPlugs

9.3.1 Miniplug mechanics and MCPMTs

The estimated cost of the mechanics and MCPMT's for the two MiniPlugs is given in Table 5. Funding for these items will be provided by the Rockefeller University. Some remaining design time needed for MiniPlug support details is estimated by our CDF engineer to be about one man-week, and the time for installation in the collision hall two man-weeks. Thanks to re-use of existing pulleys the cost of support materials is expected to be less than $5000.

Table 5: MiniPlug Mechanics and MCPMTs

	Quantity	Unit Price	Cost	Funding Source
Lead/Al plate	70	438	30,660	
Frame/Flanges			7,000	
Fibers Kuraray Y11	5,000	2	10,000	
Total Mechanics			**47,660**	
Hamamatsu R5900-M16	36	1,518	**54,648**	
TOTAL			**102,308**	**Rockefeller**

9.3.2 Miniplug front-end electronics

Each MiniPlug has 252 channels viewed by 18 16-channel MCPMTs. Each MCPMT is equipped with an output, which provides the pulse height sum of its 16 channels. The sum outputs will be read out with plug electronics. The estimated cost associated with reading out these 36 channels, 18 for each MP, is presented in Table 6.

Table 6: MiniPlug Front-End Electronics

	Quantity	Unit Price	Cost	Funding Source
CAFE card	36	120	4,320	
ADMEM board	2	3,200	6,400	
ADMEM transition module	2	300	600	
VME Crate (complete)	1	16,700	16,700	
Signal Cables	36		2,000	
HV Cables	36		2,000	
CAEN card A932N	2	1,300	2,600	
Inverters	36	25 (?)	900	
TOTAL Front-End			**35,520**	**Rockefeller**

9.4 Cost summary

Proposal

- Re-install Roman Pot Spectrometer
- Install BSCs
- Install MiniPlugs and read out the 36 MCPMT sum-outputs

Detector	Cost	Funding Source	$ Amount	Remaining
RPS	189,485	Tsukuba (Roman Pots)	150,000	39,485
BSC	40,260	Rockefeller (existing PMTs) ITEP	20,000 10,000	10,260
MP	137,828	Rockefeller	137,828	
TOTAL	**367,573**	Outside sources	**317,828**	**49,745**

Summary:

TOTAL Cost: $ 367,573

Funded by outside sources: $ 317,828

Remark: Rockefeller is optimistic about raising some more funds to cover a portion of the remaining cost of $ 49,745.

10 Manpower

The responsibility for this project will be shared by three Institutions: Fermilab, ITEP and Rockefeller. ITEP will be responsible for the BSC's, Rockefeller for the MiniPlugs, and all three Institutions for the re-installation of the RPS.

The following people will contribute to the manpower effort required:

- Fermilab
  - Michael Albrow (physicist)
  - Craig Moore (physicist)
- ITEP
  - Andrei Rostovtsev (physicist)
  - Sergei Tchechelnitsky (physicist)
  - Viacheslav Zakharov (engineer)
- Rockefeller
  - Dino Goulianos (faculty)
  - Stefano Lami (faculty)
  - Michele Gallinaro (postdoc)
  - Mary Convery (postdoc)
  - New position (postdoc)
  - Kenichi Hatakeyama (student)
  - Andrea Bocci (student)
  - Vadim Sherman (machinist)

References

[1] K. Goulianos, Phys. Lett. **B 358** (1995) 379; *ib.* **B363** (1995) 268.
K. Goulianos and J. Montanha, Phys. Rev. **D59** (1999) 114017.

[2] K. Goulianos, Proceedings of the 5th International Workshop on Deep Inelastic Scattering and QCD (DIS-97), Chicago, USA, 14-18 April 1997.

[3] L. Alvero *et al.*, Phys. Rev. D **59**, 074022 (1999).

[4] F. Abe *et al.*, Phys. Rev. **D50** (1994) 5518.

[5] F. Abe *et al.*, Phys. Rev. **D50** (1994) 5535.

[6] F. Abe *et al.*, Phys. Rev. **D50** (1994) 5550.

[7] F. Abe *et al.*, "Observation of Diffractive W-Boson Production at the Fermilab Tevatron", Phys. Rev. Lett. **78** (1997) 2698.

[8] F. Abe *et al.*, "Measurement of Diffractive Dijet Production at the Fermilab Tevatron", Phys. Rev. Lett. **79** (1997) 2636.

[9] F. Abe *et al.*, "Dijet production by color-singlet exchange at the Fermilab Tevatron", Phys. Rev. Lett. **80** (1997) 1156.

[10] F. Abe *et al.*, "Events with a Rapidity Gap between Jets in $\bar{p}p$ Collisions at $\sqrt{s} = 630$ GeV, Phys. Rev. Lett. **81** (1998) 5278.

[11] F. Abe *et al.*, "Observation of Diffractive b-quark Production at the Fermilab Tevatron", submitted to Phys. Rev. Letters.

[12] A. Solodsky, CDF Collaboration, "Observation of Diffractive J/Ψ Production at the Fermilab Tevatron", APS Meeting, Atlanta, Georgia, March 1999.

[13] "Diffractive Production at Collider Energies I: Soft Diffraction and Dino's Paradox", Chung-I Tan, hep-ph/9706276.

[14] J. D. Bjorken, Phys. Rev. **D47** (1993) 101.

[15] A. Akopian and P. Melese, "Search for DχC and Centauro Events", CDF Note 3271 (July 1995).

[16] P. Melese, "Search for Centauro Events in CDF", XI Hadrons in Collision Workshop (PBARP96), Padova, Italy, May 1996.

[17] K. Goulianos, Symp. On Very High Energy Cosmic Ray Interactions, Ann Arbor MI, (1992), RU92/E-39; Comm. on Nucl. and Part. Phys. **17**, 195 (1987).

[18] M. Church, private communication.

[19] S. Bagdasarov and K. Goulianos, *"Beyond the Plug Upgrade (***PAD:** *a* **P***ixel* **A***rray* **D***etector for the forward region of CDF in Run II)"*, CDF Note 2237.

[20] S. Bagdasarov and K. Goulianos,
"Calorimetric tracking of high energy particles", Presented by K. Goulianos, Proceedings of the Fourth International Conference on Calorimetry in High Energy Physics, La Biodola, Isola d'Elba, Italy, 19-25 September 1993, World Scientific (Aldo Menzione and Angelo Scribano, Eds.) pp.524-529.

[21] S. Bagdasarov, K. Goulianos, A. Maghakian and Q. Wang,
"Test-beam Results of a Miniplug Calorimeter Prototype", CDF Note 2867.

[22] Qingfang Wang, *"Pixel Array Detector for Forward Calorimetry"*,
V*th* International Conference on Calorimetry in High Energy Physics,
Brookhaven National Laboratory, September 25–October 1, 1994.

[23] S. Bagdasarov, K. Goulianos, A. Maghakian and Q.F. Wang,
"Test-beam results of a prototype position sensitive towerless calorimeter",
Nucl. Instrum. Meth. **A 372** (1995) 117-124.

[24] K. Goulianos, S. Lami and A. Solodsky,
"Miniplug Calorimeter Performance at the 1997 CDF Test Beam", CDF Note 4279.

[25] K. Goulianos and S. Lami,
"Performance of a Prototype Position Sensitive Towerless Calorimeter at the 1997 CDF Test Beam",
Presented by S. Lami, Proceedings of the Seventh International Conference on Calorimetry in High Energy Physics, Tucson, Arizona, 9-14 November 1997.

[26] K. Goulianos and S. Lami,
"Proposed Forward Detectors for Diffractive Physics in CDF-II",
Presented by K. Goulianos at "Diffractive Physics, LAFEX International School on High Energy Physics (LISHEP-98), Rio de Janeiro, Brazil, 10-20 February 1998"; CDF Note 4548; FERMILAB-CONF-98/111-E.

[27] K. Goulianos and S. Lami,
"Performance of a prototype position sensitive towerless calorimeter", Nucl. Instrum. Meth. **A 430** (1999) 34-47.

[28] "Proposal to CDF for Run II: Further Studies in Hard Diffraction and Very Forward Physics", August 20, 1997, CDF Note 4591.

[29] K.G. Young et al., 'Radiation and Solvent Effects on WLS Fibers used with Liquid Scintillators', Proc. of the Int. Conf. on Radiation–Tolerant Plastic Scintillators and Detectors, Radiation Physics and Chemistry **41** (1993), 215.

[30] Stefano Lami, *"Study of the CDF MiniPlug Calorimeter Optical System"*, CDF Note 4361 (1997).